Norsk Regnesentral
NORWEGIAN COMPUTING CENTER

Statens vegvesen

NGI

Note

Evaluation of automatic detection of avalanches in high-resolution optical satellite data

Results from the ESA avalRS project's feasibility study on automated avalanche detection

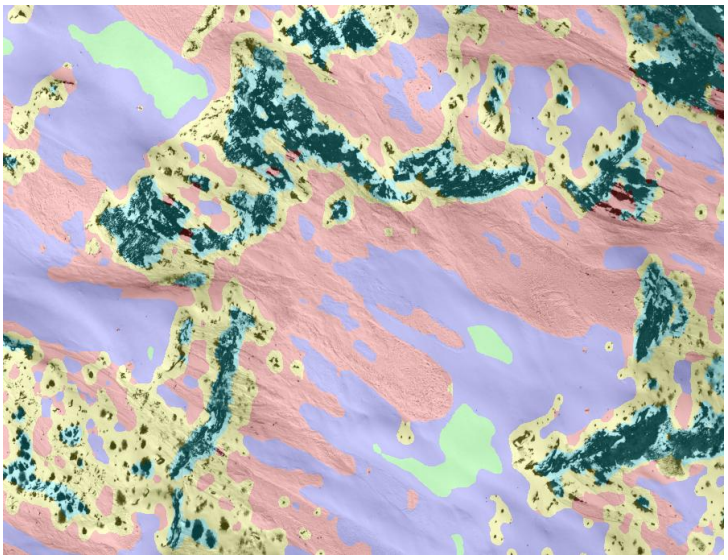

Note no: SAMBA/23/11

Authors: Siri Øyen Larsen, Arnt-Børre Salberg and Rune Solberg

Date: 05 July 2011

Contract: ESRIN/Contract No. 22139/08/I-EC

Norsk Regnesentral

Norsk Regnesentral (Norwegian Computing Center, NR) is a private, independent, non-profit foundation established in 1952. NR carries out contract research and development projects in the areas of information and communication technology and applied statistical modelling. The clients are a broad range of industrial, commercial and public service organizations in the national as well as the international market. Our scientific and technical capabilities are further developed in co-operation with The Research Council of Norway and key customers. The results of our projects may take the form of reports, software, prototypes, and short courses. A proof of the confidence and appreciation our clients have for us is given by the fact that most of our new contracts are signed with previous customers.

Norges Geotekniske Institutt

NGI (Norwegian Geotechnical Institute) is a leading international centre for research and consulting in the geosciences. NGI develops optimum solutions for society, and offers expertise on the behaviour of soil, rock and snow and their interaction with the natural and built environment. NGI works within the oil, gas and energy, building and construction, transportation, natural hazards and environment sectors. NGI is a private foundation with office and laboratory in Oslo, branch office in Trondheim and daughter company in Houston, Texas, USA. NGI was awarded Centre of Excellence status in 2002 and leads the International Centre for Geohazards (ICG).

NGI is the prime contractor of the project behind the work presented in this report.
Address: Norwegian Geotechnical Institute (NGI), P.O. Box 3930 Ullevaal Stadion, NO-0806 Oslo, Norway
Contact person: Regula Frauenfelder (regula.frauenfelder@ngi.no)

Norwegian Public Road Administration

The Norwegian Public Roads Administration (NPRA) is responsible for the planning, construction and operation of the national and county road networks, vehicle inspection and requirements, driver training and licensing. It is also authorized to grant subsidies for ferry operations. The Public Roads Administration is under the leadership of the Directorate of Public Roads, which is an autonomous agency subordinated the Ministry of Transport and Communication. The Public Roads Administration encompasses five regional offices.

Address: Norwegian Public Road Administration. P.O. Box 8142 Dep. NO-0033 Oslo, Norway
Contact person: Heidi Bjordal (heidi.bjordal@vegvesen.no)

Norsk Regnesentral
Norwegian Computing Center
Postboks 114, Blindern
NO-0314 Oslo, Norway

Besøksadresse
Office address
Gaustadalléen 23
NO-0373 Oslo, Norway

Telefon · telephone
(+47) 22 85 25 00
Telefaks · telefax
(+47) 22 69 76 60

Internett · internet
www.nr.no
E-post · e-mail
nr@nr.no

Title	**Evaluation of automatic detection of avalanches in high-resolution optical satellite data**
Authors	**Siri Øyen Larsen, Arnt-Børre Salberg and Rune Solberg**
Quality assurance	Rune Solberg
Date	05 July 2011
Year	2011
Publication number	SAMBA/23/11

Abstract

The AvalRS project has previously demonstrated that avalanches could be successfully detected and mapped from high resolution optical satellite imagery. The key part of this first version of a detection algorithm is a texture segmentation step, which distinguishes the avalanches from other objects such as smooth and rugged snow, trees and rock.

The aim of this report is to evaluate the performance of our initial algorithm on a larger dataset. In addition to one new dataset covering Norwegian terrain, we have analyzed two datasets covering Swiss terrain. One of the Swiss datasets consists of aerial images, as opposed to the QuickBird satellite images otherwise used.

Keywords	Avalanche mapping, texture, Quickbird, aerial images
Target group	Remote sensing researcher, avalanche researchers, road authorities
Availability	Open
Project number	220 438
Research field	Earth observation
Number of pages	32

Contents

1 Introduction

The main objective of the avalRS project is to provide the Norwegian Public Roads Authority with avalanche inventories based on remote sensing data captured briefly after major avalanche events. The service is to be demonstrated in specific service case areas defined on-the-fly (i.e. depending on where major avalanche events will occur during the project phase) within the mountains of South-, West- and Central Norway.

AvalRS aims at demonstrating that such a service is possible and that it will provide decision support during avalanche-imposed road closures, and to help validate the issued avalanche forecasts. Overview over the affected problem area, specifically the length of the avalanche-affected road section and the volume of snow on the road, are essential for the authorities during road closures.

The avalRS project is a joint project between the Norwegian Geotechnical Institute (prime contractor), the Norwegian Computing Center (sub-contractor) and the Norwegian Public Roads Authority (end-user). The project is funded by the ESA DUE (Data User Element) Innovator II programme (Contract No. 22139/08/I-EC).

To detect and map the avalanches, we have demonstrated two different texture segmentation methods; one based on gray-level co-occurrence matrices (GLCM) (Haralick et al., 1973) and one based on directional filters (Varma and Zisserman, 2004). In our previous project report (Larsen et al., 2010) we presented the results of applying these two strategies on two QuickBird images (from Hellesylt and Dalsfjorden, both locations in Norway). We concluded that both the GLCM and directional filter approaches were able to extract potential avalanche areas. The segmentation results indicated that the GLCM approach extracted the boundaries better than the directional filter approach, but struggled to separate sparse trees from avalanches. One of the strengths of the directional filter approach seemed to be that it was able to separate sparse trees from avalanches well.

In this report we will present results from running the directional filter algorithm on three additional data sets: QuickBird images form Eikesdalsvatnet (Norway) and Val Gronda (Switzerland), as well as aerial images from Davos (Switzerland). We will first briefly recapitulate the methods (Section 2), which are explained in detail in the previous report (Larsen et al., 2010). We then present the evaluation data set (Section 3) and experimental results (Section 4), before we evaluate the performance and discuss necessary improvements together with potential solution strategies (Section 5). In Section 6 we will draw some conclusions.

NGIs role in this part of the project has been to identify datasets suitable for evaluation, make manual outlines of avalanches (groundtruth), perform orthorectification, and evaluate the results. NRs contribution has been to prepare the data for input to the pattern recognition algorithm (which was developed by NR in the first stage of the project), run the processing, and evaluate the results.

2 The methodological approach

In other projects with similar type of challenges, i.e., automated object detection from satellite images, we have obtained good results using an approach consisting of image segmentation into objects, followed by feature extraction and classification (Figure 2-1). Examples include oil spill detection in SAR images (Solberg et al., 2007), and detection of cultural heritage sites (Trier et al., 2009) or vehicles (Larsen et al., 2009) in high-resolution optical images. We propose using a similar approach for automated avalanche detection and mapping. Each processing step must be adjusted to meet the requirements for object recognition of the specific type, here the objects are avalanches.

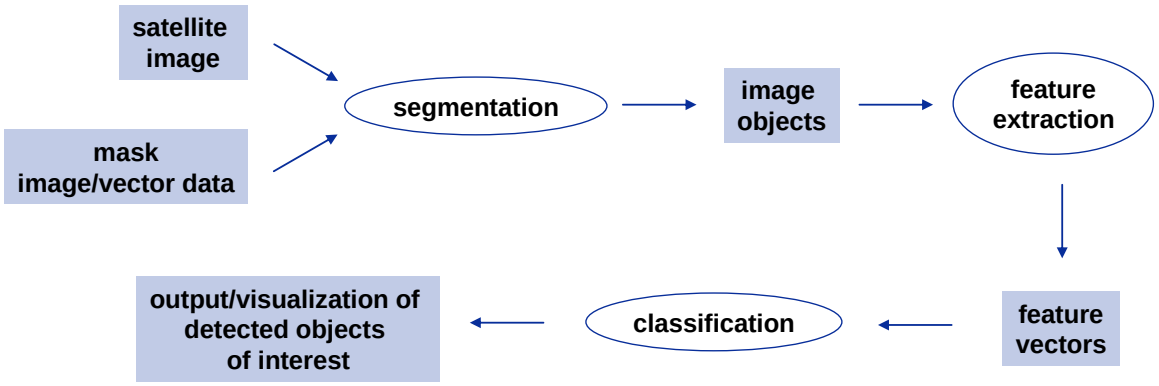

Figure 2-1. Processing flow of the general approach.

The segmentation strategy used here is based on extraction of textural features from the image. We apply different filters - contained in a filter bank - to the image by convolution. Each filter represents a certain type of texture at some characteristic scale and orientation. Then, given a single-band image, its filter responses can be combined into a multi-dimensional image, which is further analyzed to stratify the image into segments with similar texture patterns.

Our approach is based on the so-called MR8 filter bank suggested by Varma and Zisserman (2004), which consists of 38 filters: an edge and a bar filter, each at six orientations and three scales, as well as a Gaussian and a Laplacian of Gaussian filter (Figure 2-2). Considering only the maximum response across orientations reduces the number of responses from 38 (six orientations at three scales for two oriented filters, plus two isotropic) to eight (three scales for two filters, plus two isotropic) - hence the name (MR8) of the filter bank.

The depositional area of an avalanche is often characterized by high roughness due to deposition and compression of big chaotically arranged snow chunks, while in its upper part, the avalanche typically results in a texture pattern that has linear structures in the same direction as the aspect of the hill side. We have therefore modified the MR8 filter bank approach by selecting the same orientation of the bar and edge filters as the aspect of the DEM. Furthermore, since trees and tree shadows are oriented vertically in the image, we extend the MR8 filter bank by including six filters with vertical orientation (bar and edge filters, each at three different scales). Hence, our resulting texture segmentation is based on a 14 dimensional image. The selected scale parameters are (1.5, 3.0, 6.0) and (0.5, 1.0, 2.0) for the major and minor axis of the directional filters. The scale parameter for the isotropic filters is 5.0.

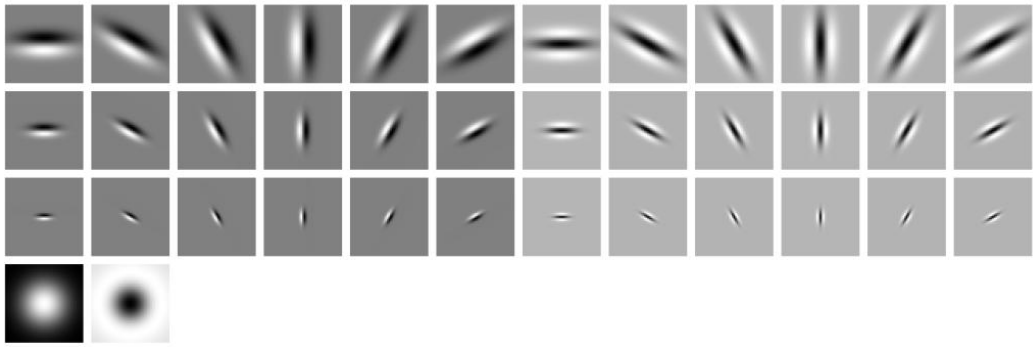

Figure 2-2. The MR8 filter bank. The figure is taken from Varma and Zisserman (2004).

The general approach consists of a learning stage and a classification stage. In the learning stage, we select a set of image example areas - regions of interest (ROIs) - to represent each texture class. For our application we have defined five classes: *avalanche, smooth snow, rugged snow, sparse trees,* and *rock*. We then find a set of *textons*, which can be seen as example filter responses, by clustering the filter responses corresponding to the same class using K-means, and choosing the resulting cluster means as textons. All the textons from all the classes are then collected in a texton dictionary. We use K=10 and five classes, hence the texton dictionary consists of 50 textons. Next, each pixel in the training areas are labelled by classifying each pixel to one of the textons in the dictionary using a maximum likelihood classifier based on a Gaussian distribution. The histogram of texton frequencies is then used to form *models*. From the training ROIs we create a model data base, which can be used for classification of the whole image (from which the training ROIs were selected), and of course also for new images. I.e., for each pixel of an image to be classified, we select a local neighbourhood, map the pixels onto textons (from the dictionary learnt during training), compute the histogram and compare it with the models from the data base learnt during training. To compare the models, a nearest neighbour classifier is used and the χ^2 statistic is employed to measure the distances. The histograms are normalized to sum to unity.

Figure 2-3 illustrates one of the strengths of using directional filters in our application. Typically, the avalanche is enhanced by applying the aspect directional filters, whereas sparse trees are suppressed. By applying the vertical directional filters, we obtain the opposite effect.

For each potential avalanche region from the segmentation module, several shape, intensity, and context based features may be extracted, and the regions may then be classified using a suitable classifier. We will not discuss this topic further here, but refer to our previous report (Larsen et al., 2010), where we sketched some ideas regarding what sort of features to extract and how to perform object based classification in order to rule out marked objects with low confidence.

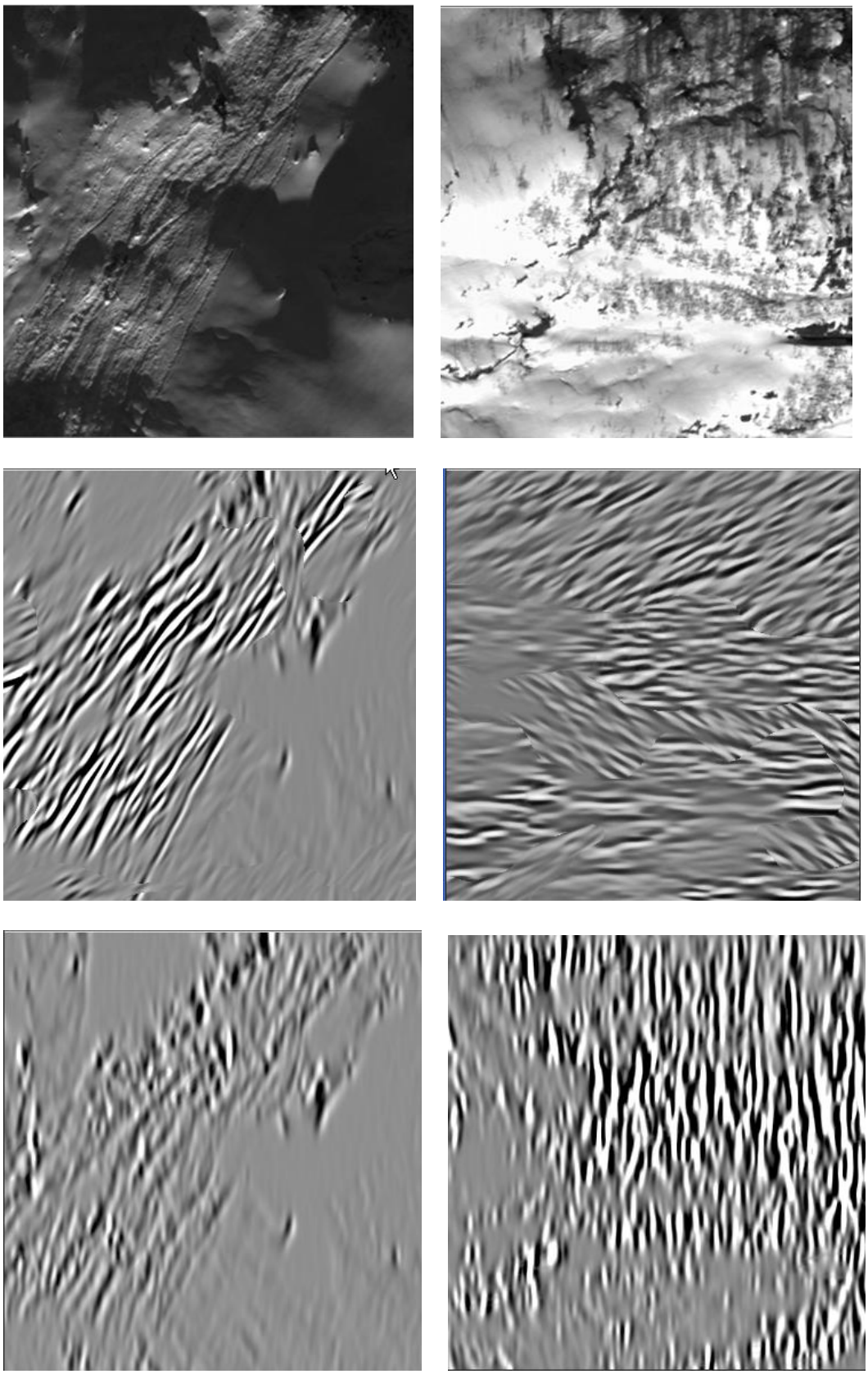

Figure 2-3 Left figures: Filter responses of a typical avalanche (upper left) filtered with a directional filter along the aspect direction (mid figure left) and vertical direction (lower left). Right figures: Typical sparse forest area (upper right) filtered with directional filter along the aspect direction (mid figure right) and vertical direction (lower right).

3 Evaluation data sets

3.1 Image data

In this report we evaluate the performance of the avalanche detection approach discussed previously on three datasets (see also Frauenfelder, 2011). The three datasets consist of:

1. A QuickBird panchromatic image (0.6m resolution) from the area around **Eikesdalsvatnet** in Møre og Romsdal county in western, central Norway, acquired April 13, 2011 (Figure 3-1).

   This image contains several old, partially melted avalanches, with deposits in the forest, while the avalanche paths are concentrated along streams and gullies. There are also some fresh avalanches in the higher areas, although the illumination conditions in these areas of the image makes manual detection difficult.

2. A QuickBird panchromatic image (0.6m resolution) from **Val Gronda** in the canton of Grisons, Eastern Switzerland, acquired February 25, 2009 (Figure 3-2).

   This scene contains many smaller avalanches, but not many that are fresh. There are also quite a lot of old avalanches possibly covered with newly fallen snow or partially eroded that can be seen as disturbances in the snow surface, but that have not been mapped manually.

3. Aerial images from an ADS 50 S42 airborne camera covering the greater **Davos** area in Switzerland. Original ground resolution for the images is 0.2m. The avalanche detection algorithm assumes the input image to have 0.6m resolution (i.e., QuickBird resolution) and contain a panchromatic band only, but since the Davos images have an original ground resolution of 0.2m, they were resampled accordingly, using pixel aggregation. We also selected one of the four bands (red, green, blue, and NIR) at the time for processing.

   The Davos dataset is courtesy of Leica-Geosystems (Heerbrugg, Switzerland) and Dr. Yves Bühler (WSL Institute for Snow and Avalanche Research SLF) and has been thoroughly analyzed by Bühler (2009) and Bühler et al. (2009). This dataset is to be used within the avalRS project exclusively and must not be used in another study or be given to a third party without explicit permission by Leica-Geosystems.

   We have selected five image sections for analysis, which will be referred to as Davos A (Figure 3-3), B (Figure 3-4), C (Figure 3-5), D (Figure 3-6), and E (Figure 3-7).

3.2 Orthorectification

All images have to be orthorectified before input to the avalanche detection algorithm, since it is dependent on the aspect information in each pixel. Datasets 3 had already been orthorectified by Leica-Geosystems, using a DEM with 25 m resolution from the Swiss Federal Office of Topography. For data set 1 (the Eikesdalsvatnet image) we initially tried to perform orthorectification using a built-in module in ENVI together with manually selected ground control points and a 15 m DEM. However, the process did not yield satisfactory results, as the image contained wavelike distortions in several areas. These effects may be caused by the poor resolution of the DEM, and/or conditions in the orthorectification module, which acts as a

"black box", i.e., we do not have access to the details on how the image is processed. Instead, NGI orthorectified the image using PCI Geomatica. The image still contains some "problem areas", i.e., areas with distortions due to incomplete information during orthorectification, and this should be taken into account when evaluating the processing results of the avalanche detection algorithm on the image. Dataset 2 was also orthorectified by NGI within PCI Geomatica.

3.3 Ancillary data

As already mentioned above, the avalanche detection algorithm is dependent on the aspect information in each pixel, in order to select the corresponding orientation for the oriented filters in the texture segmentation step (cf. Section 2). The aspect orientation is calculated from the DEM, resampled to match the geographic coordinates of the image pixels. For datasets 2 and 3 we used DEMs with an original resolution of 25 m, while the DEM used for dataset 1 has 15 m resolution.

3.4 Training data

The avalanche detection methods were developed on a QuickBird image from Hellesylt in Møre og Romsdal county in Norway (i.e., from the same part of the country as the Eikesdalsvatnet image) acquired on April 16, 2005. The texton dictionary and model data base were extracted from this image (Larsen et. al, 2010) and used as training data for the evaluation images.

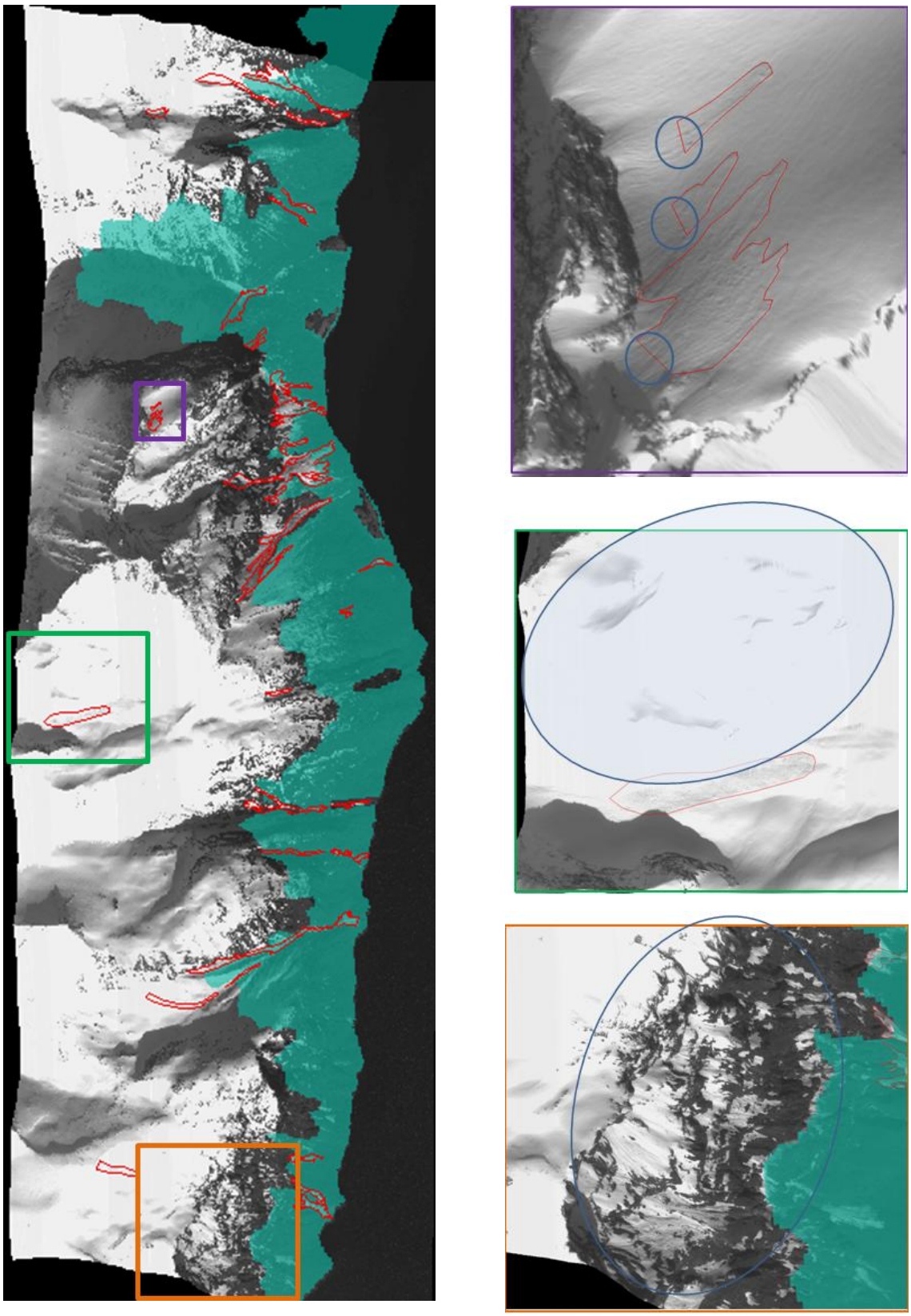

Figure 3-1 On the left, the Eikesdalsvatnet image, with forest mask (green) and manually mapped avalanches (red outlines) overlaid. Purple box/upper right: the blue circles show release areas that could not be mapped with high enough certainty visually. Green box/middle right: circled area may contain avalanches, but is not possible to map by visual inspection due to too high illumination intensities. Orange box/lower right: circled area contains many old avalanche paths that have not been mapped since their depositional areas are all masked out by the forest mask. Source: NGI.

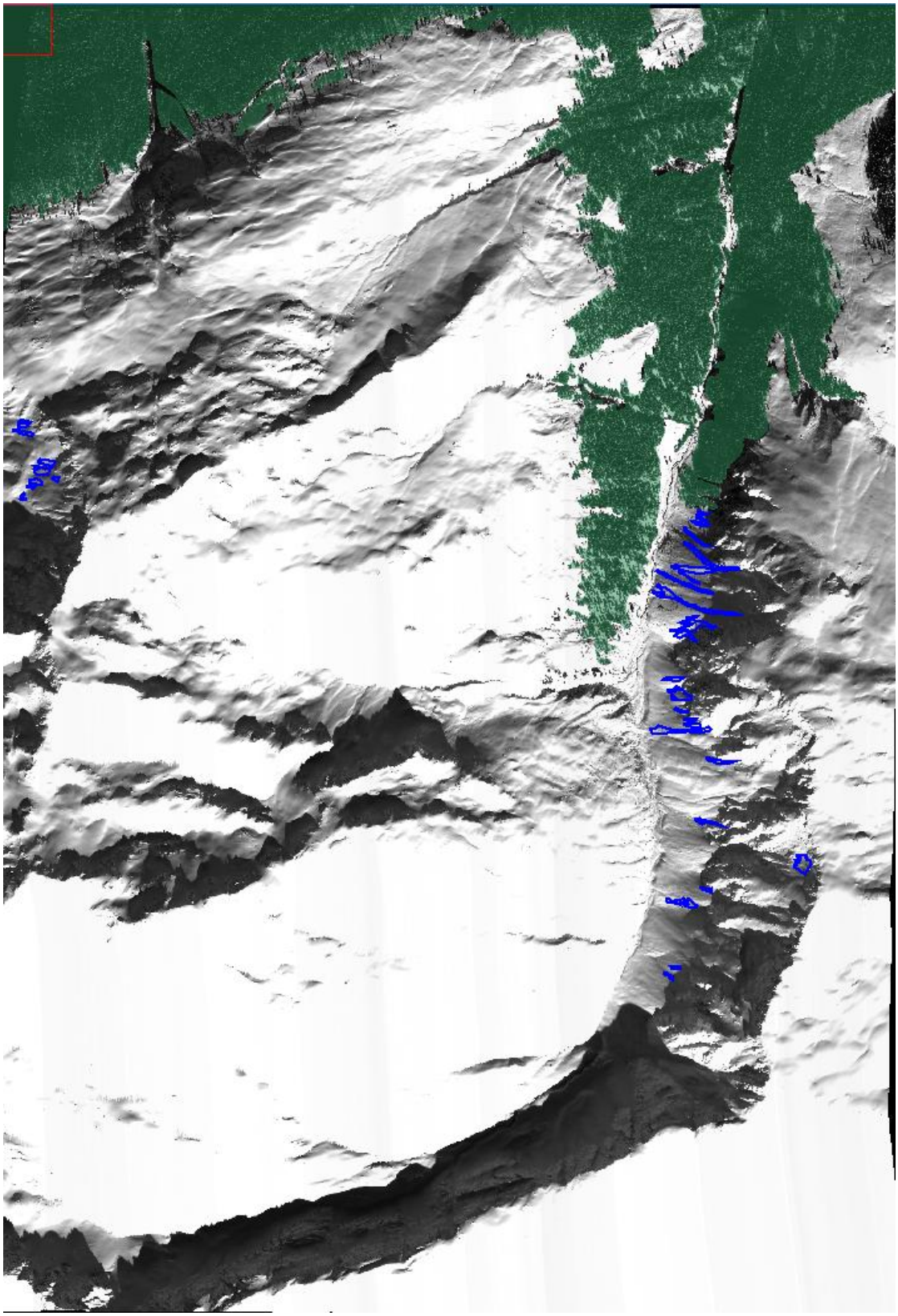

Figure 3-2 The Val Gronda image, with manually mapped avalanches outlined in blue, and forest mask (green overlay). Source: NGI.

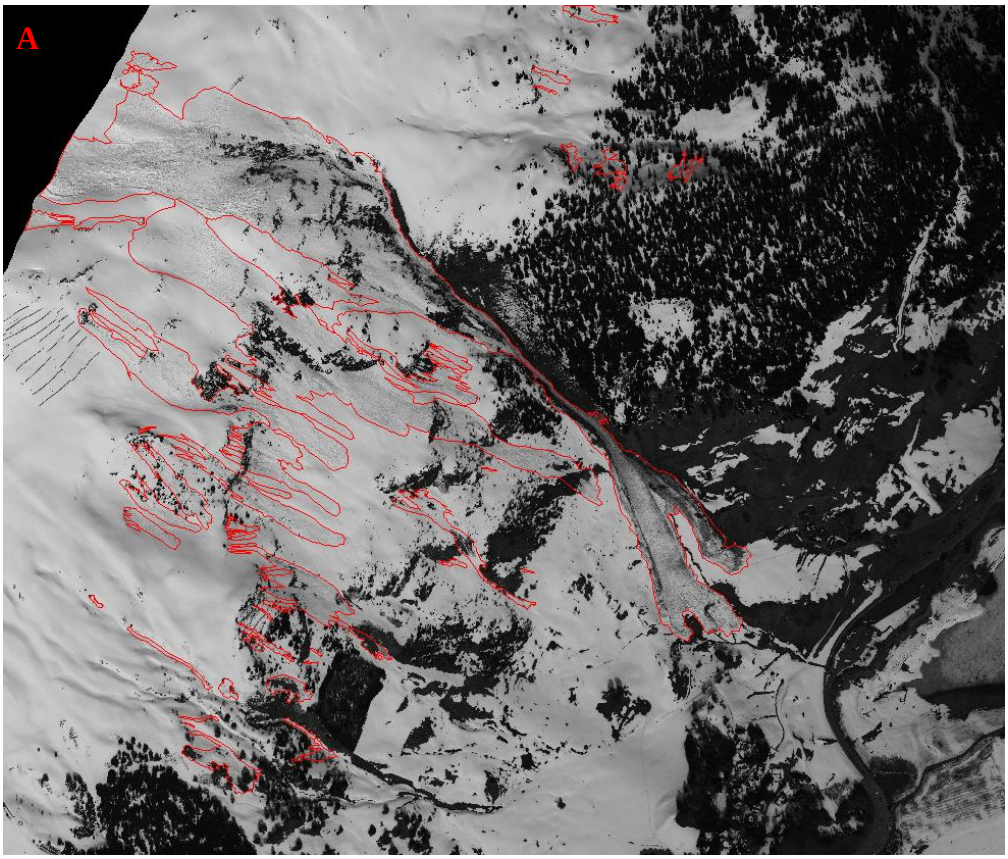

Figure 3-3 Davos image A (red band resampled to QuickBird resolution) with manually mapped avalanches outlined in red. Sources: Image: © Leica-Geosystems (Heerbrugg, Switzerland) and Dr. Yves Bühler (Davos, Switzerland); Avalanche outlines: NGI.

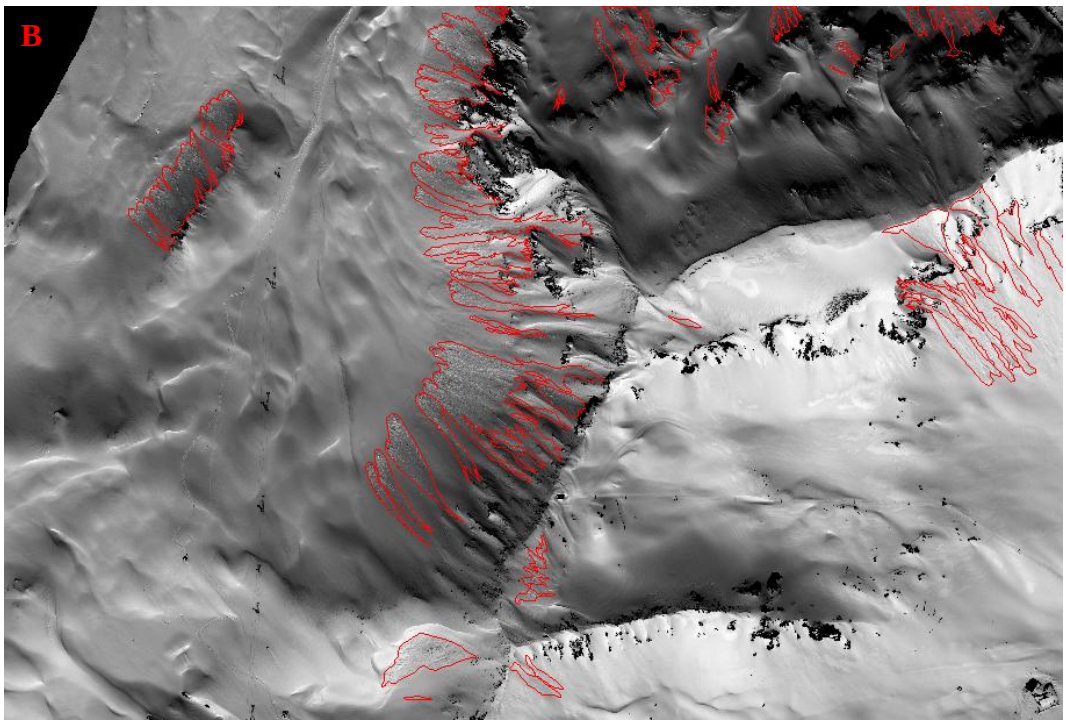

Figure 3-4 Davos image B (red band resampled to QuickBird resolution) with manually mapped avalanches outlined in red. Sources: Image: © Leica-Geosystems (Heerbrugg, Switzerland) and Dr. Yves Bühler (Davos, Switzerland); Avalanche outlines: NGI.

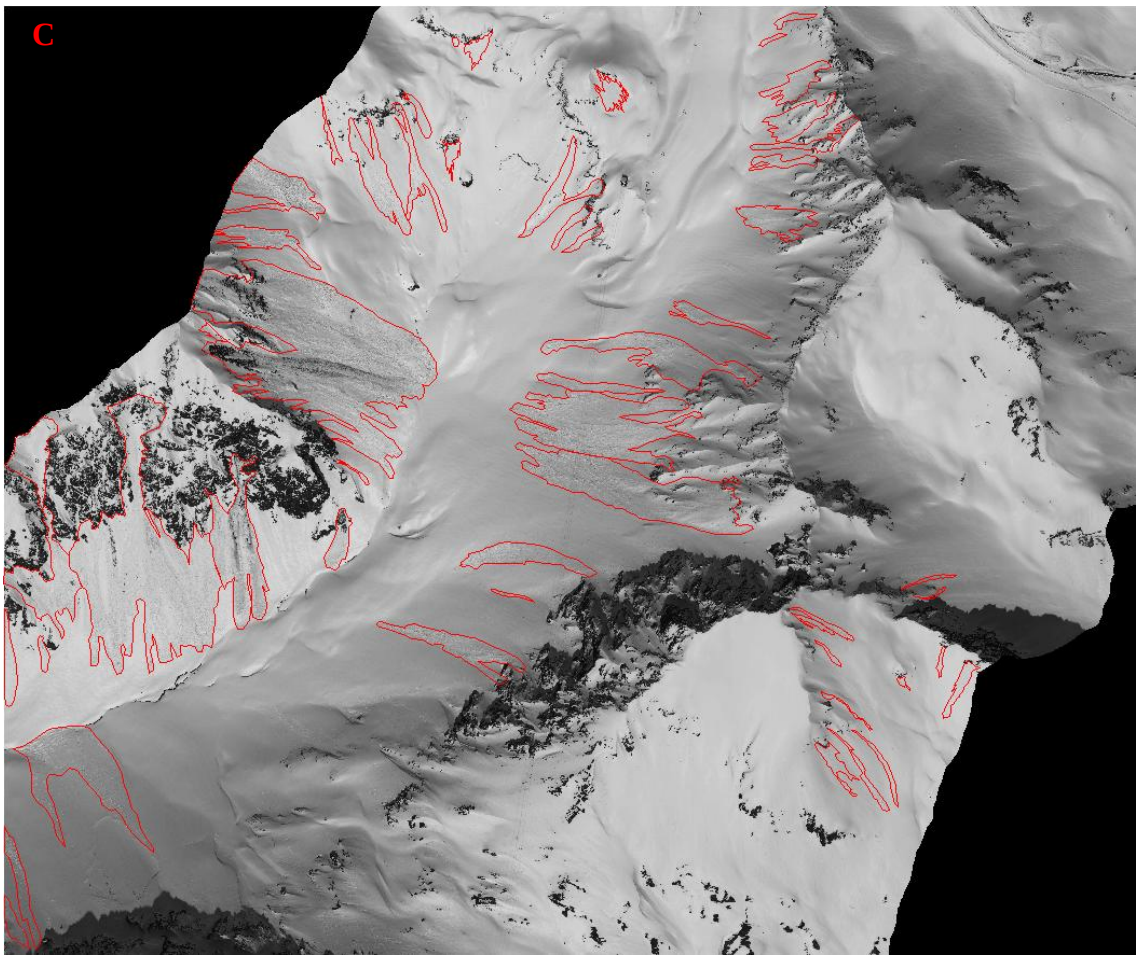

Figure 3-5 Davos image C (red band resampled to QuickBird resolution) with manually mapped avalanches outlined in red. Sources: Image: © Leica-Geosystems (Heerbrugg, Switzerland) and Dr. Yves Bühler (Davos, Switzerland); Avalanche outlines: NGI.

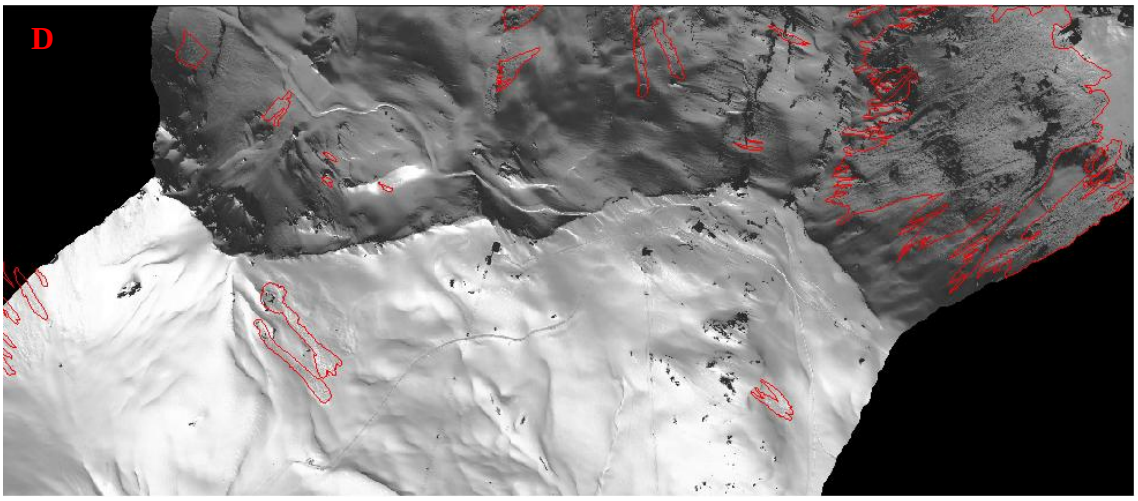

Figure 3-6 Davos image D (red band resampled to QuickBird resolution) with manually mapped avalanches outlined in red. Sources: Image: © Leica-Geosystems (Heerbrugg, Switzerland) and Dr. Yves Bühler (Davos, Switzerland); Avalanche outlines: NGI.

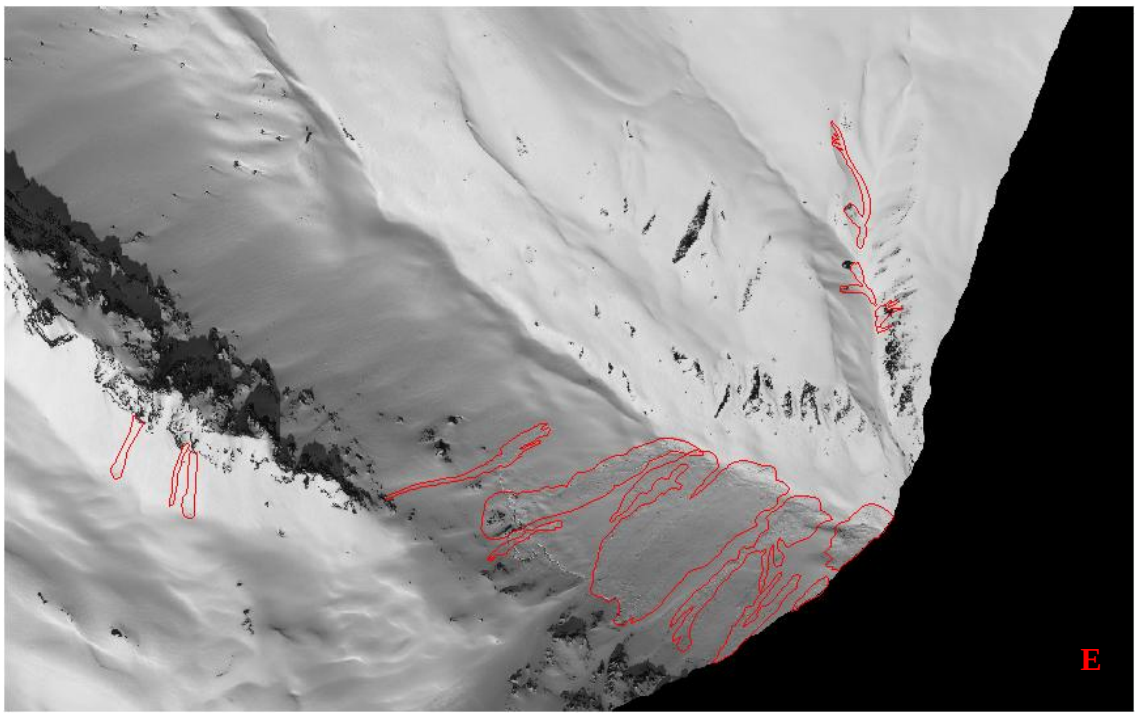

Figure 3-7 Davos image E (red band resampled to QuickBird resolution) with manually mapped avalanches outlined in red. Sources: Image: © Leica-Geosystems (Heerbrugg, Switzerland) and Dr. Yves Bühler (Davos, Switzerland); Avalanche outlines: NGI.

4 Evaluation results

In the current section we will present the results of avalanche detection on the data sets introduced above. In addition to a figure displaying the segmentation result for the entire image, we illustrate the behaviour of the algorithm with a few close-up examples by zooming into interesting parts of the image. For the datasets from Eikesdalsvatnet and Val Gronda, we show the manually detected avalanche outlines in blue overlaid on the panchromatic image of these close-ups, and in black overlaid on the corresponding segmentation image. The segmentation result is presented as an image where the coloring represents the class label given to the corresponding pixels, using the following color chart:

- **avalanche**
- **smooth snow**
- **rugged snow**
- **sparse forest**
- **rock**

Figure 4-1 through Figure 4-5 show results for the Eikesdalsvatnet image. Since the image contains several avalanches with deposits ending up in the forest, we show only results from processing without forest mask. Note also, as mentioned above, that some portions of the image were corrupted by the orthorectification process. Results for the Val Gronda image are shown in Figure 4-6 through Figure 4-8.

The results for the Davos dataset are shown in Figure 4-9 through Figure 4-22. For simplicity, we only show results using the red band as input to the algorithm. The manually detected avalanche outlines are shown in white on top of both the intensity and segmentation images. (Note that for the Davos dataset, the segmentation result is shown as a colored layer on top of the intensity image, thus the colors look faded compared to the colors in the color chart). Trials using the different bands in turn (red, green, blue, and NIR) indicated that the red band is the one yielding the best performance for our application (the differences between the red and green bands are minor, though).

4.1 Eikesdalsvatnet results

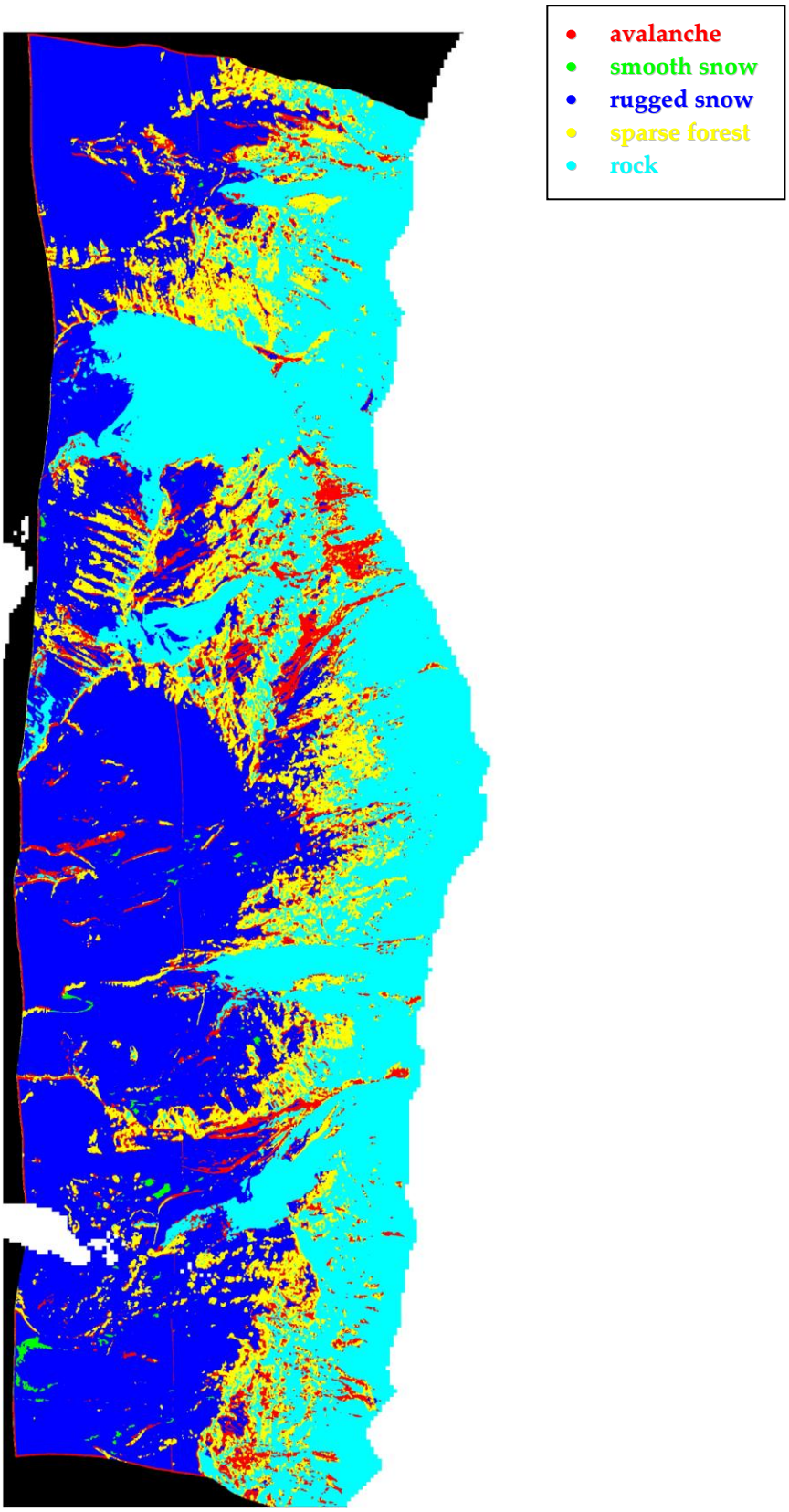

Figure 4-1 Segmentation result using the directional filter method on the Eikesdalsvatnet image (Figure 3-1). Water has been masked out in white.

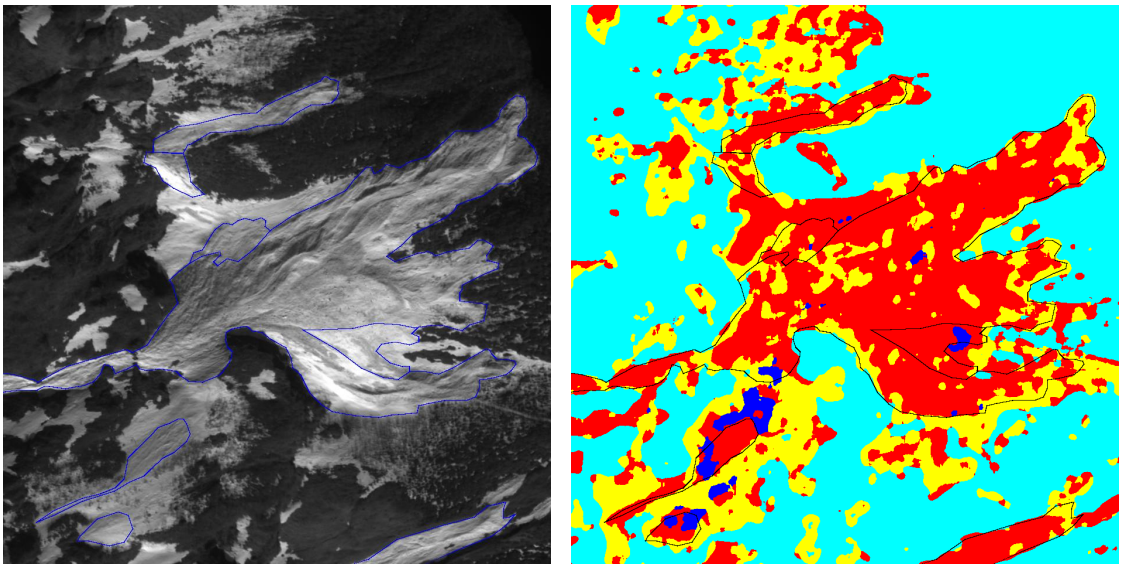

Figure 4-2 Eikesdalsvatnet / Example 1: Panchromatic image on the left, with avalanches outlined in blue, and corresponding segmentation result on the right, with avalanches outlined in black.

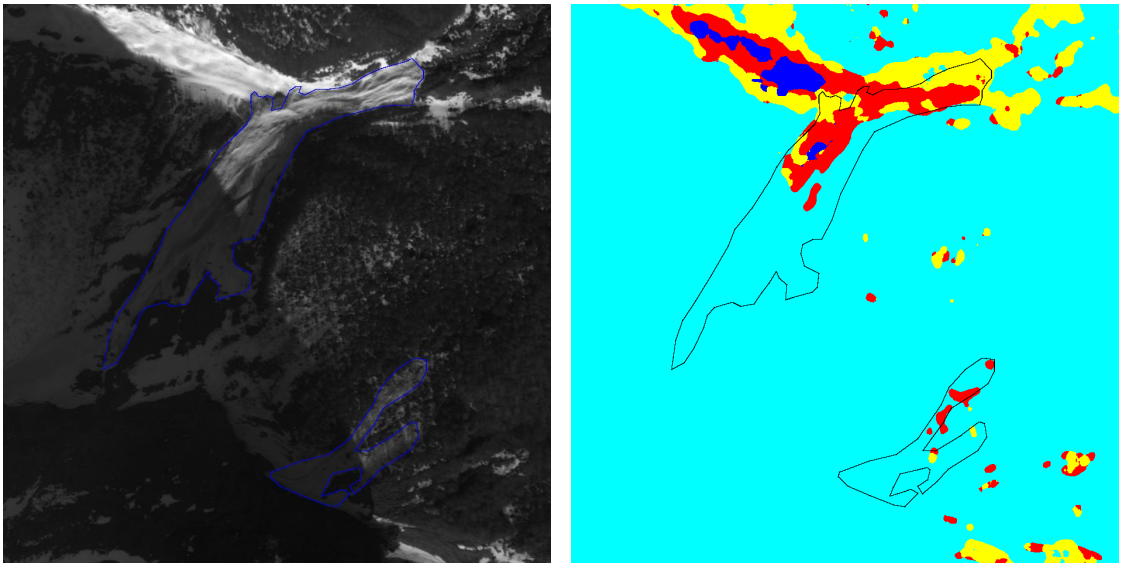

Figure 4-3 Eikesdalsvatnet / Example 2: The avalanches in this example lie partially in shadow, and large parts of the shadowed (dark) area are classified as rock. The classified avalanche towards the upper left actually does contain an old avalanche run. It had not been manually mapped because it did not contain any fresh avalanches at the time of image capture.

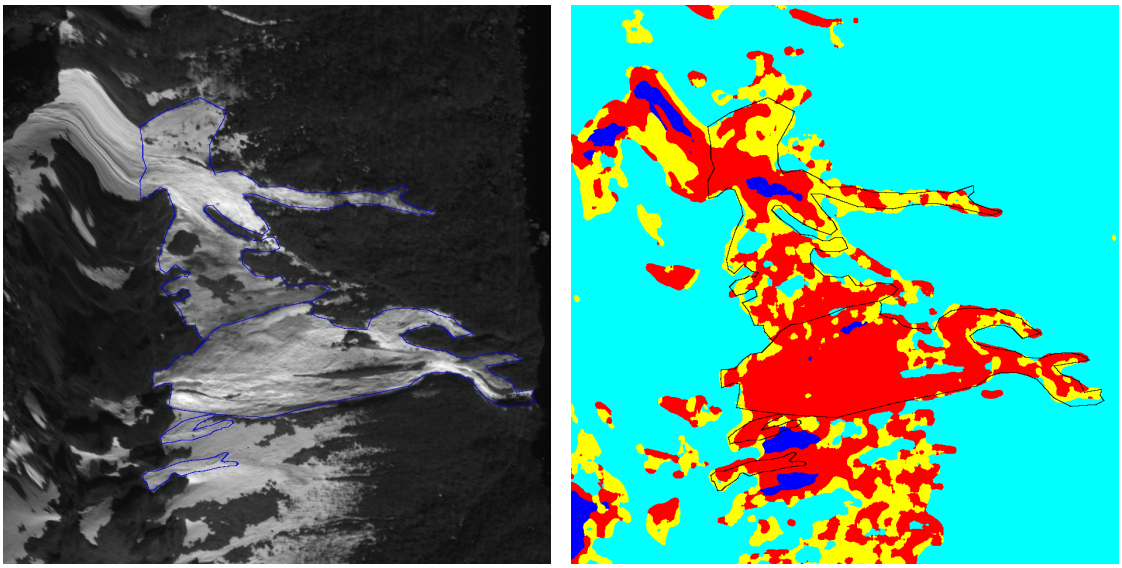

Figure 4-4 Eikesdalsvatnet / Example 3: Note the image distortions (from orthorectification) on the left in the panchromatic image, where manual mapping did not make sense.

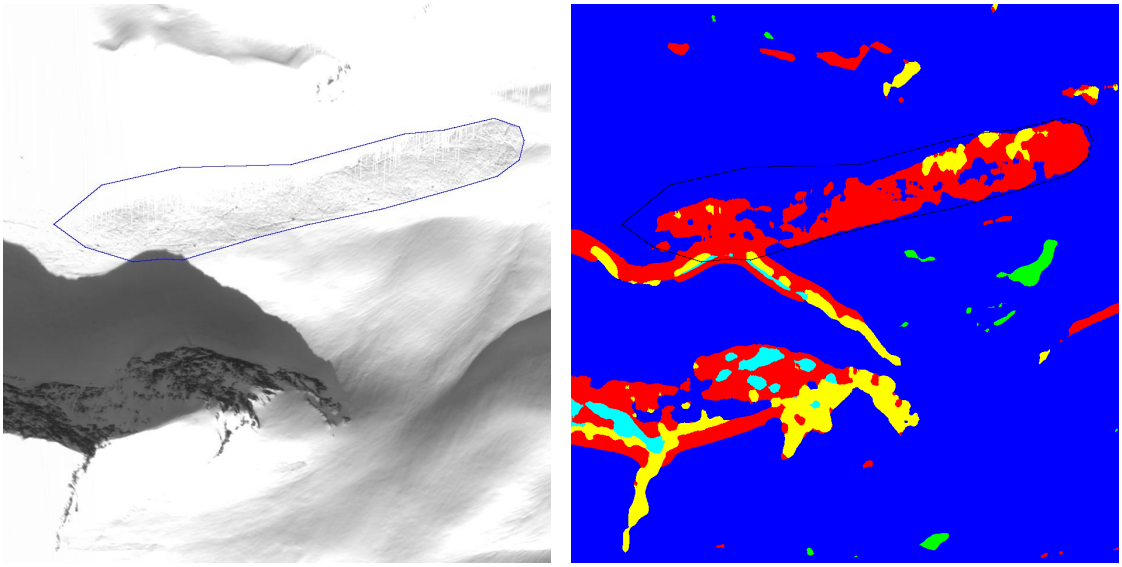

Figure 4-5 Eikesdalsvatnet / Example 4: The figure shows an avalanche in a very bright area of the image, where the texture characteristics are a bit different from the above examples. This leads to misclassification in the steep rock face and along light-shadow edges.

4.2 Val Gronda results

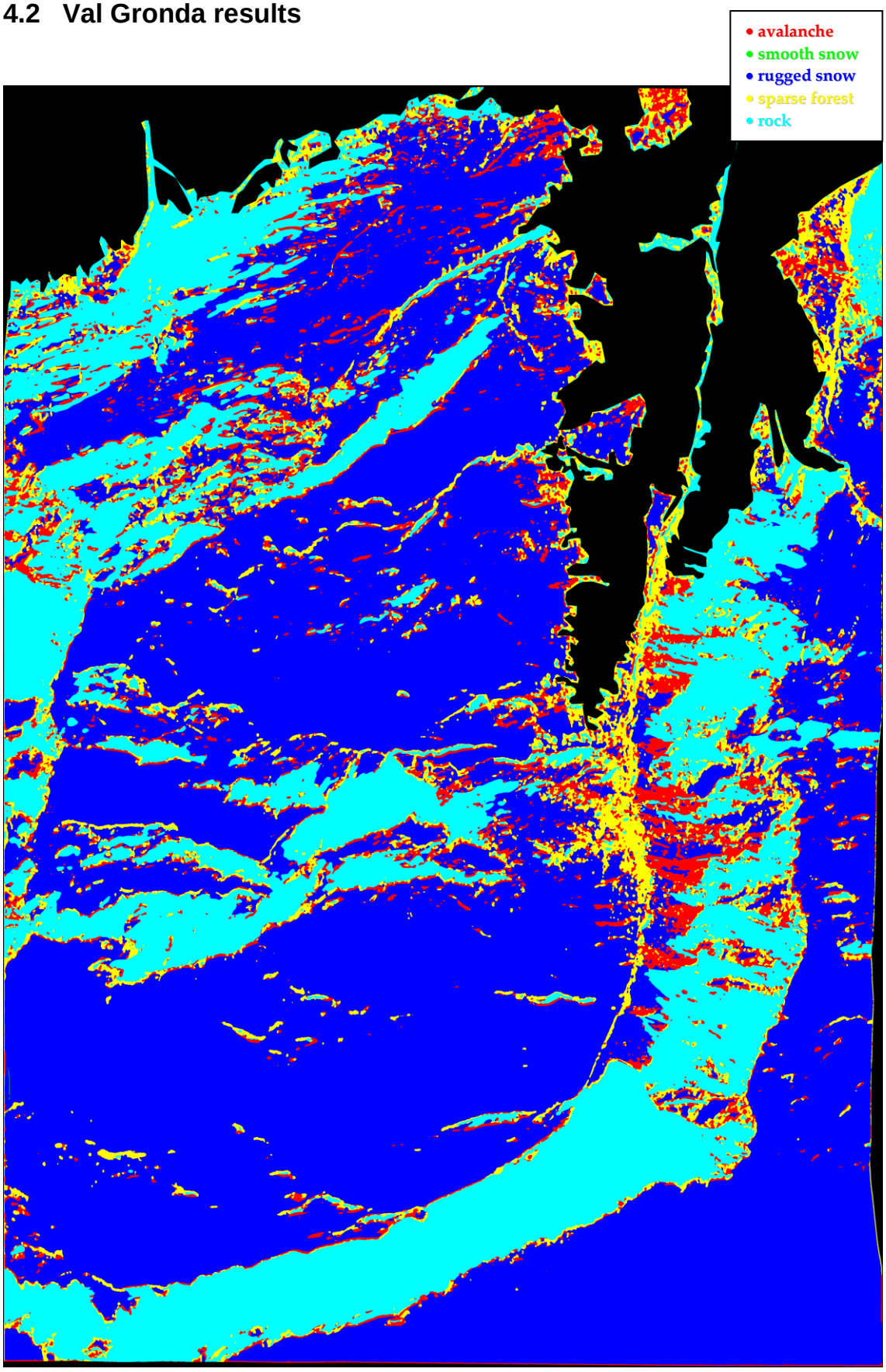

Figure 4-6 Segmentation result on the Val Gronda image (Figure 3-2), with the forest masked out.

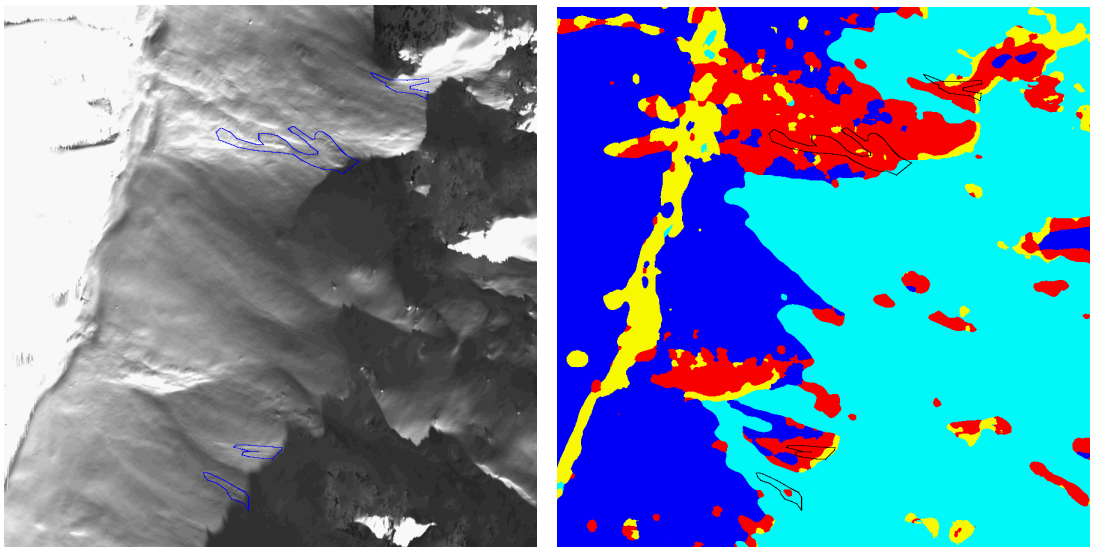

Figure 4-7 Val Gronda / Example 1: The relatively poor results in this image may be caused by the fact that the avalanches are old and the texture not as visible in the image as in the training data. Most of the larger areas classified as avalanche snow are old, partly re-worked (wind erosion, new snow layers?) avalanche deposits.

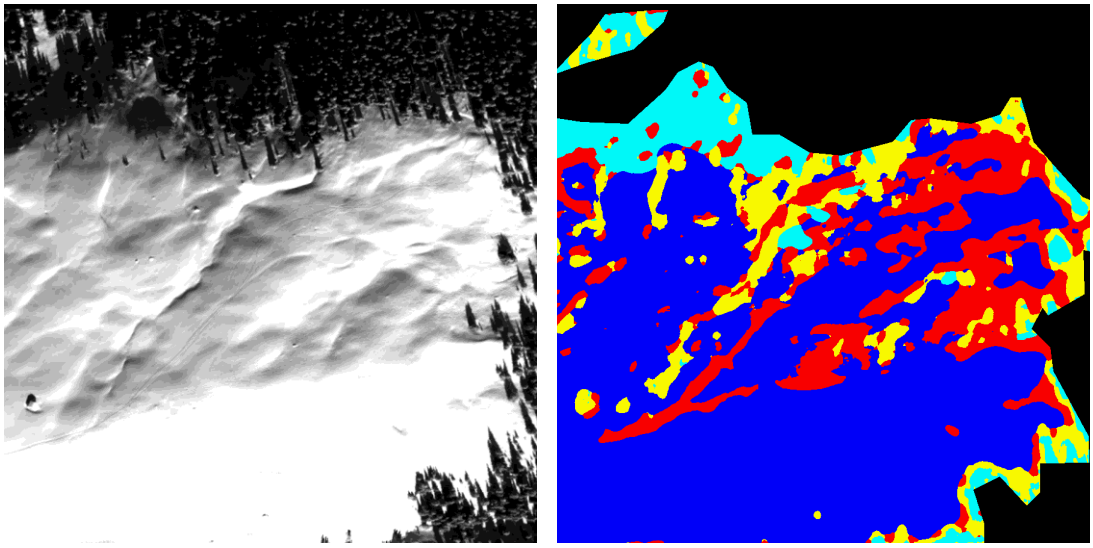

Figure 4-8 Val Gronda / Example 2: False positive avalanche. Note the rugged snow patterns (ski tracks from the lower left towards the middle right, and a creek bed from south-west to north-north-east) running more or less in the aspect direction.

4.3 Davos results

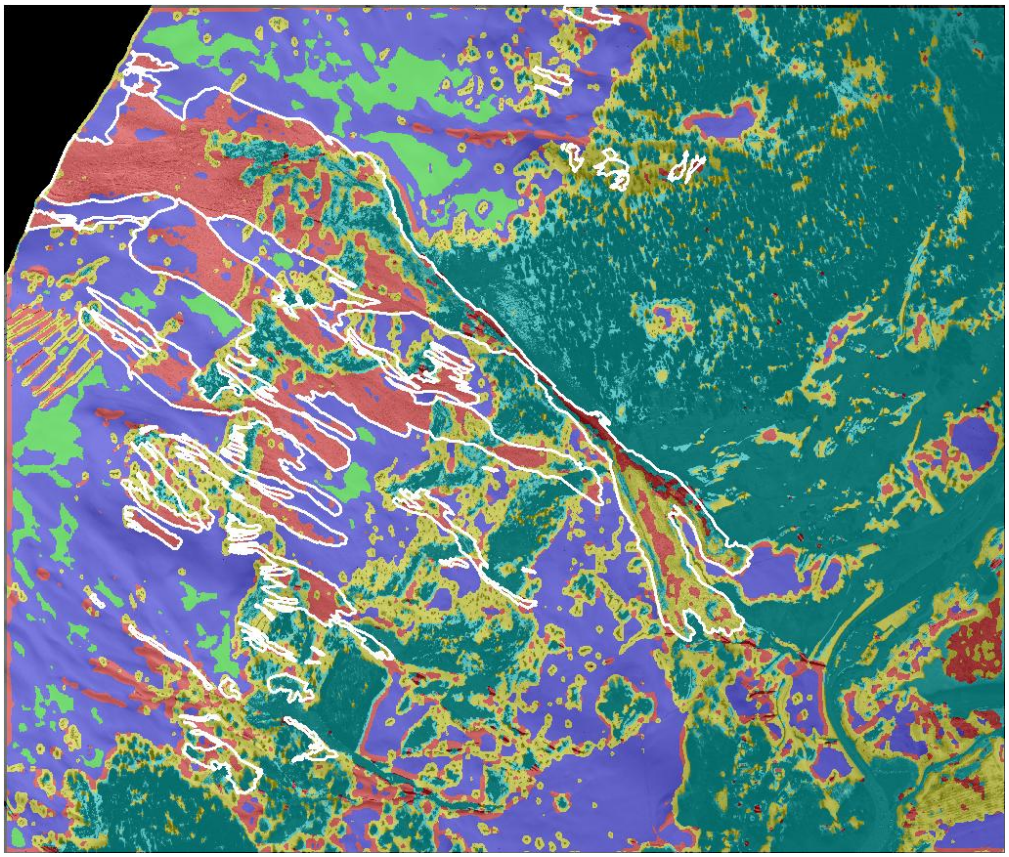

Figure 4-9 Result on Davos image A (cf. Figure 3-3).

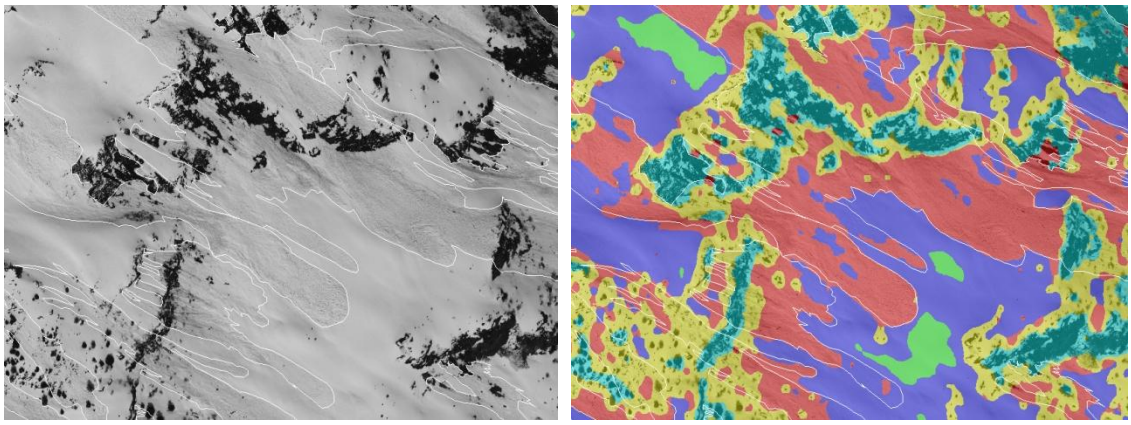

Figure 4-10 Davos image A / Example 1: The algorithm was able to successfully map the avalanches in this image.

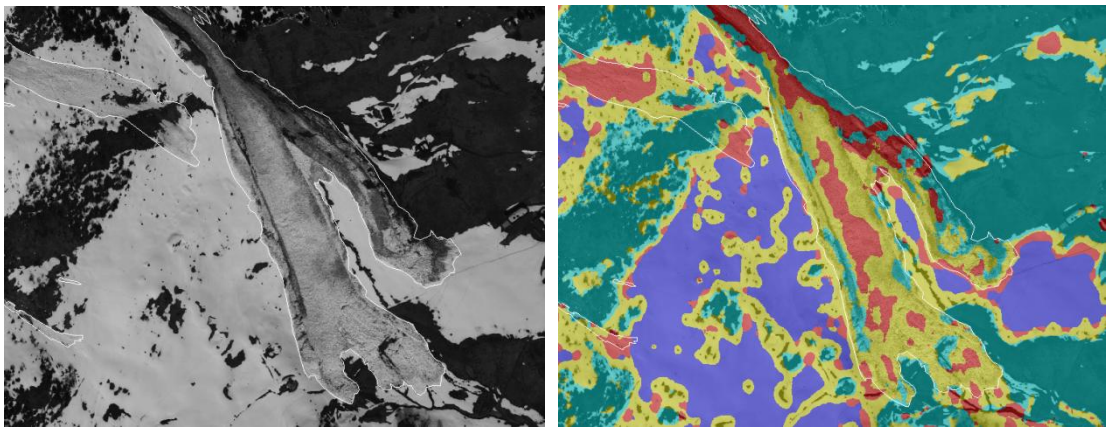

Figure 4-11 Davos image A / Example 2: The avalanche in this image is darker (because it contains rock and soil particles entrained within this large ground avalanche) than the training data, and has been partially classified as sparse trees.

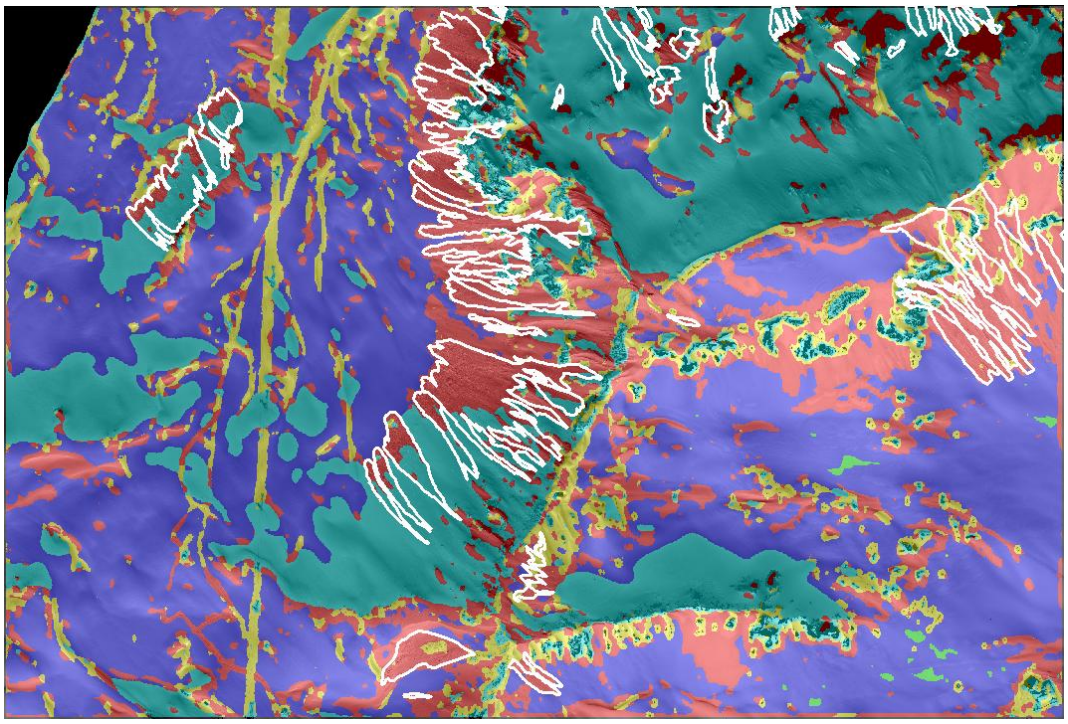

Figure 4-12 Result on Davos image B (cf. Figure 3-4).

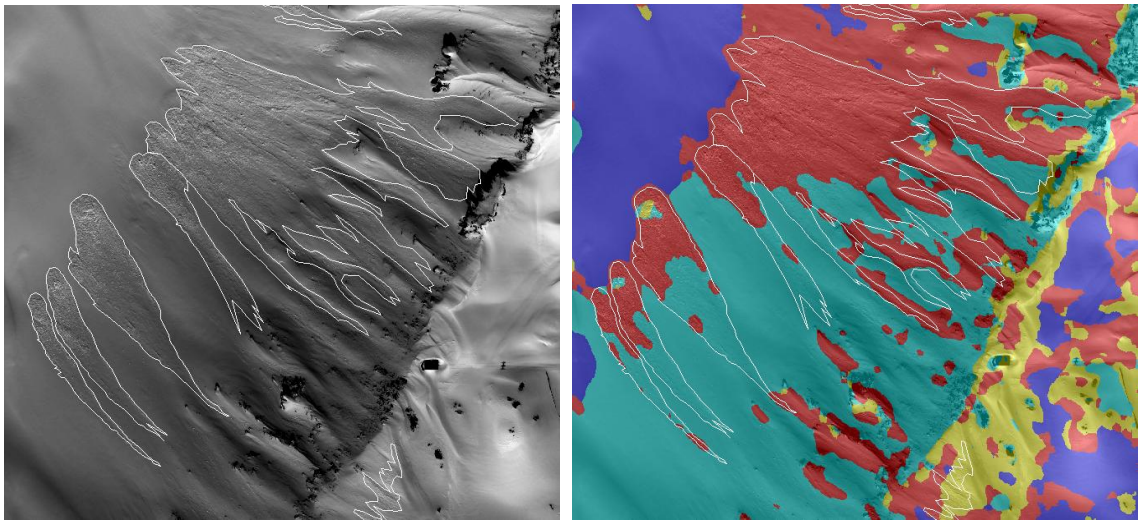

Figure 4-13 Davos image B / Example 1: The figure shows a close-up look at some of the avalanches in Davos image B and the corresponding segmentation result..

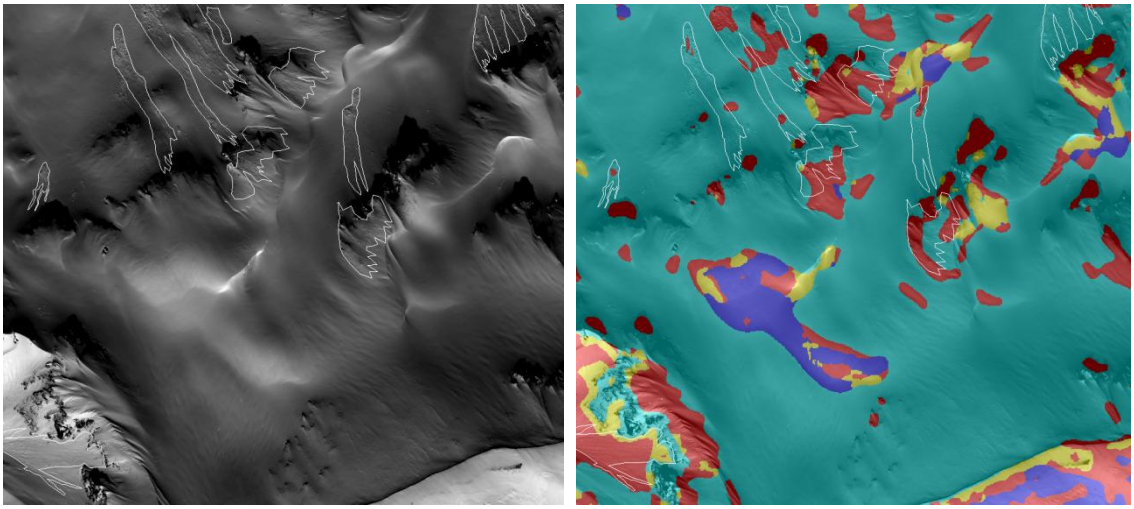

Figure 4-14 Davos image B / Example 2:Some of the smaller avalanches in an area with other disturbances are harder to detect.

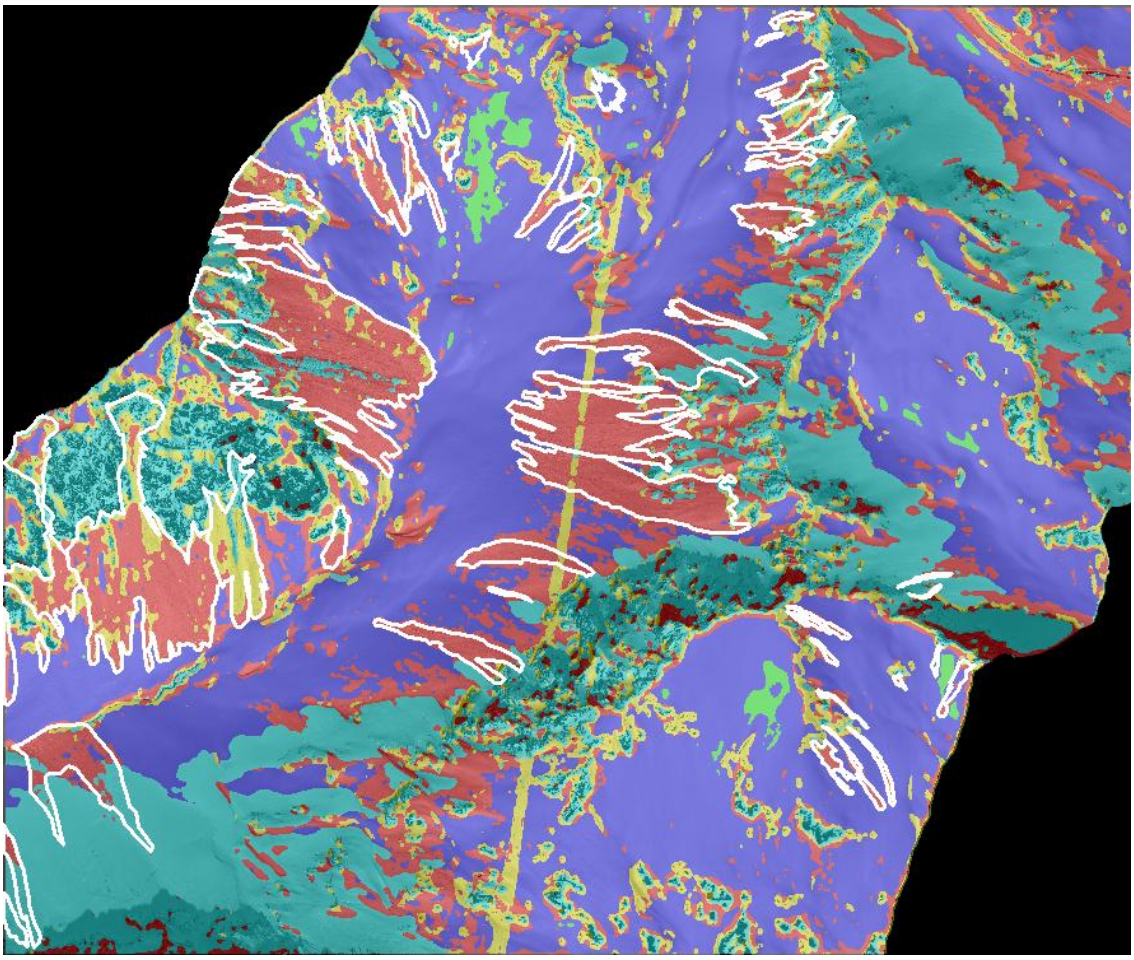

Figure 4-15 Result on Davos image C (cf. Figure 3-5).

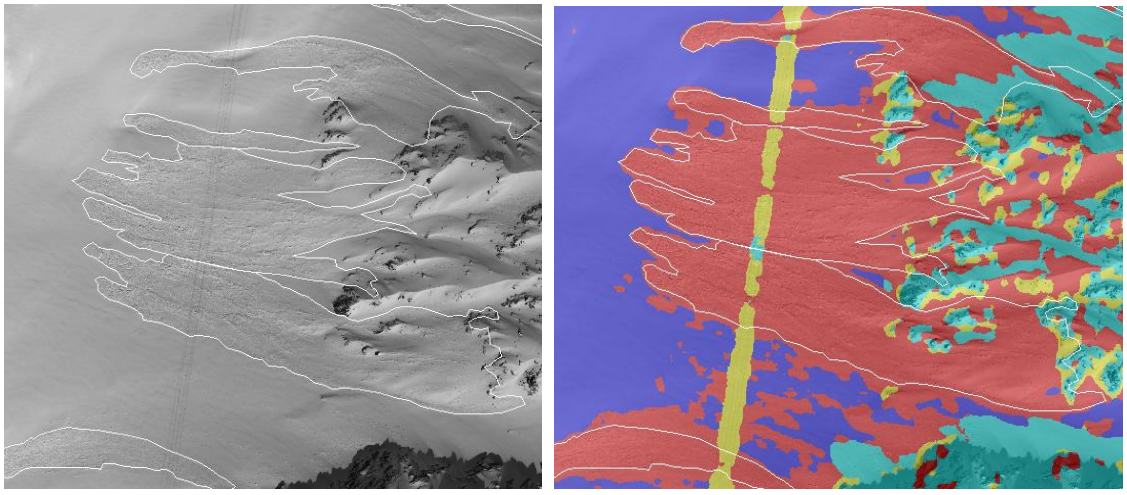

Figure 4-16 Davos image C / Example 1: The avalanche has been detected. Note the power lines in the vertical direction in the image, which have been classified as sparse forest.

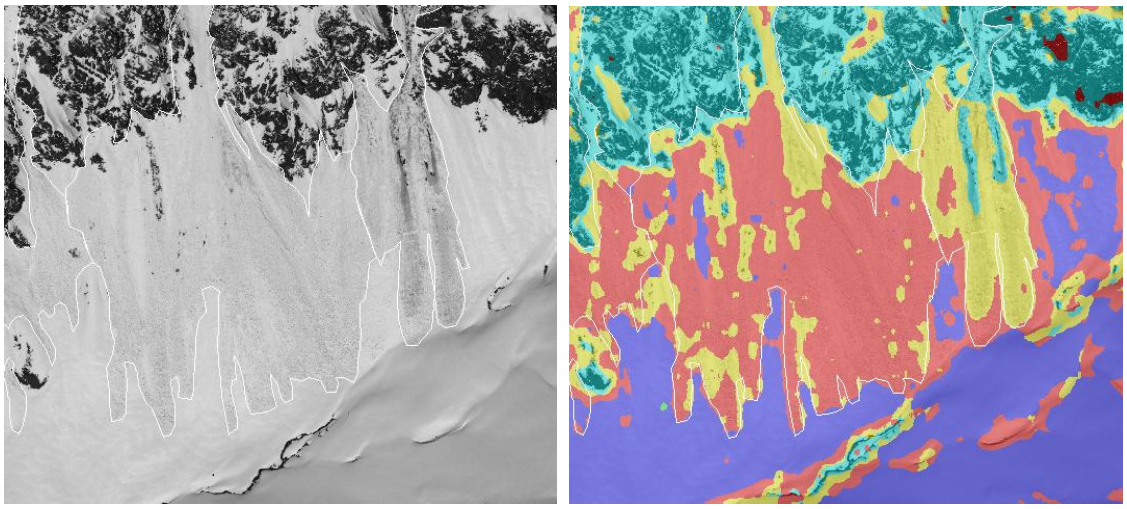

Figure 4-17 Davos image C / Example 2: In this image we see avalanches with varying intensity contrast. The darker avalanche (on the right in the image) has been classified as sparse forest.

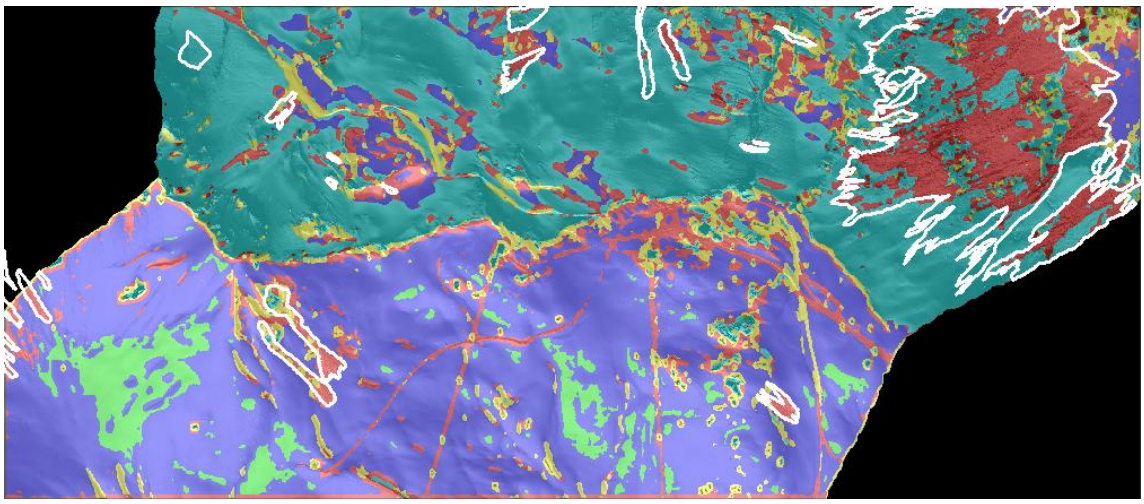

Figure 4-18 Result on Davos image D (cf. Figure 3-6).

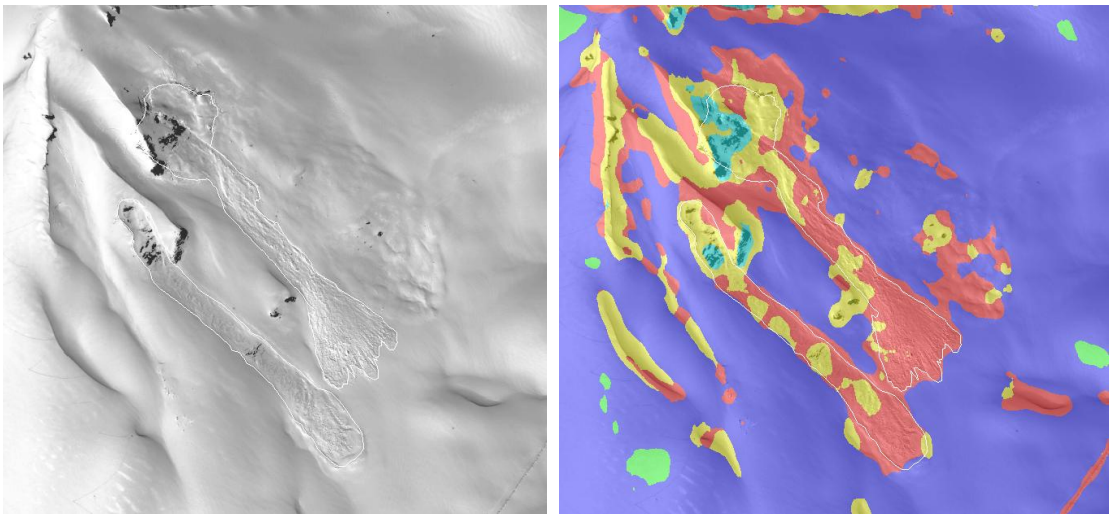

Figure 4-19 Davos image D / Example 1: The algorithm is able to map most of the fresh avalanches, while the old (topmost) avalanche in the image is only partially captured. (Note: trained only on fresh).

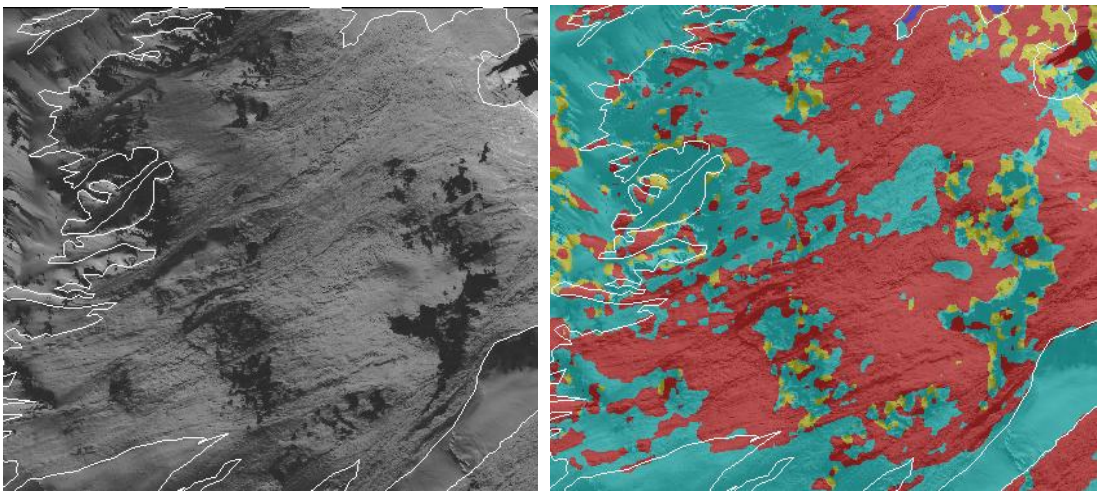

Figure 4-20 Davos image D example 2: The mapping of avalanches is rather good in image D.

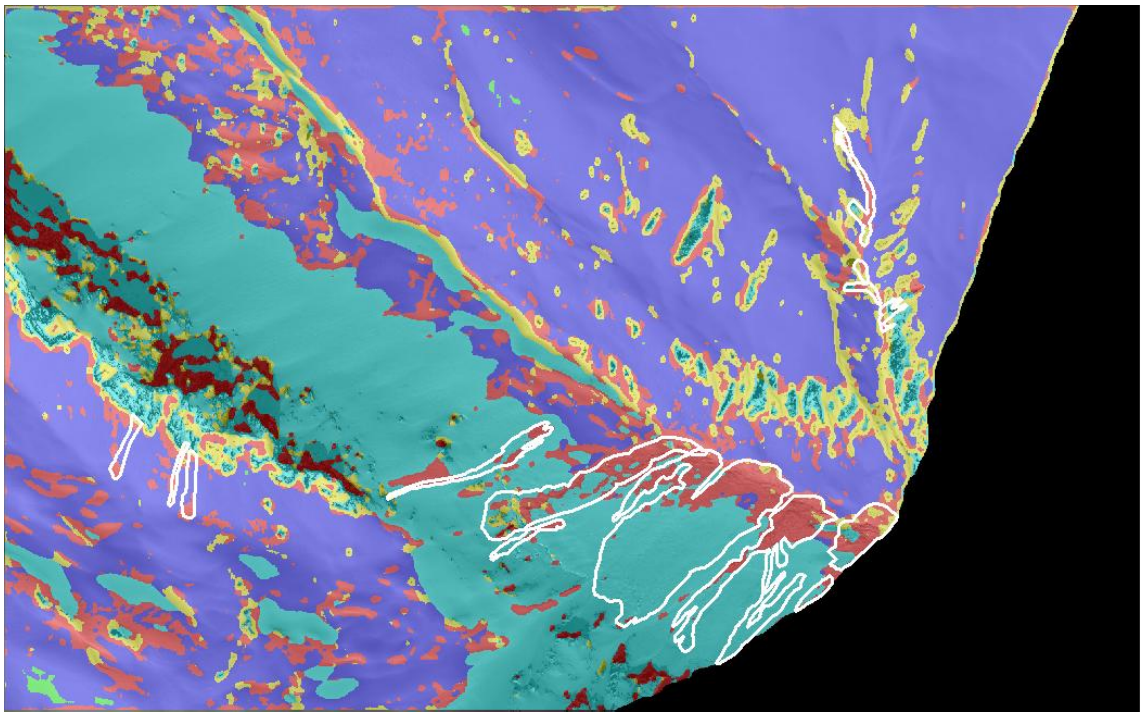

Figure 4-21 Result on Davos image E (cf. Figure 3-7).

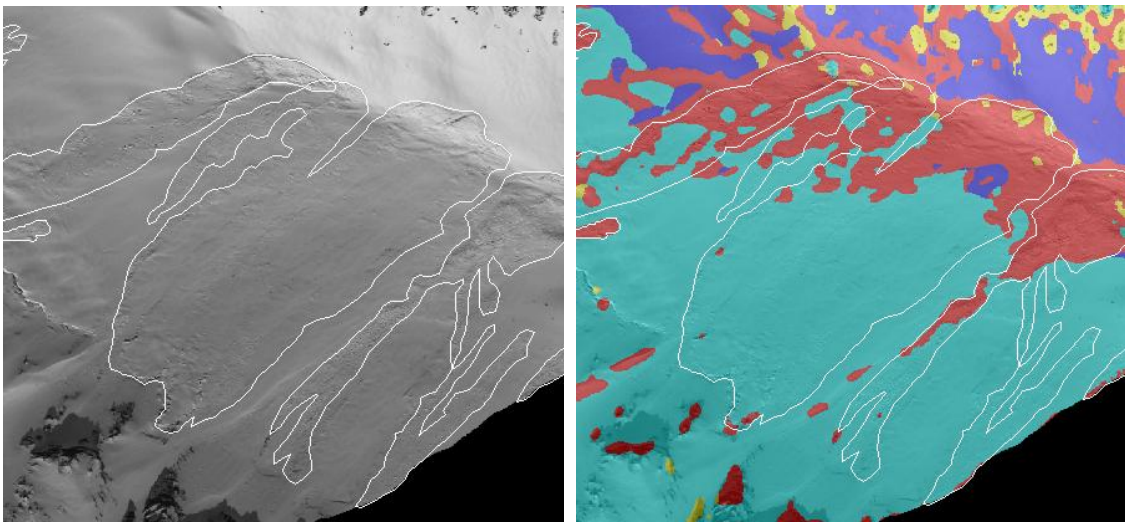

Figure 4-22 Davos image E / Example 1: The algorithm fails to detect the part of the avalanche lying in shadow.

5 Discussion and potential improvements

The presented approach, involving texture segmentation using directional filters for automatic detection of avalanches, performed in general well on the validation datasets. Although we have used a relatively small amount of training data, extracted from one Norwegian location (Hellesylt) only (Larsen et al., 2010), the analysis on the evaluation data showed that we are able to detect several avalanche regions in images with rather different conditions. However, there are still some challenges related to the segmentation, which will be discussed in the current section, in light of the close-up examples presented in the figures of section 4.

Eikesdalsvatnet / Example 1 (Figure 4-2) shows that the algorithm is able to detect the avalanche areas, although it at the same time illustrates that the extraction of the shape of the avalanche is a challenging task. A few solutions, including region growing, was discussed in our initial project report (Larsen et al., 2010), and further research needs to be conducted.

Eikesdalsvatnet / Example 2 (Figure 4-3) and Davos image E / Example 1 (Figure 4-22) illustrates how avalanche deposits lying in shadow may be missed by the detection, caused by the fact that shadow (dark) areas are often confused with the class "rock". This may indicate that the algorithm is too sensitive to the image intensity, and that intensity invariant texture properties should be considered. The method should be developed further so that detection is possible even in shadow or other dark areas.

We must perform some sort of intensity normalization of the image and the filters, but it is not straightforward how this should be done. The oriented MR14 filters are normalized to have zero mean, while the isotropic filters are not. The reasoning behind letting the isotropic filters have non-zero mean was to separate the "rock" and "smooth snow" classes in the Hellesylt image (used for algorithm development) better, since initial experiments indicated that these two "smooth" textures were often confused otherwise. However, since the final goal is to map avalanche regions and discrimination between the other classes are of minor importance, the filter normalization should be reconsidered. Furthermore, the global conditions of the image, both when it comes to illumination and landscape, also affect the classification and make the algorithm sensitive to the natural intensity variation between different images. One solution may be to perform local intensity normalization before filtering. Another answer to the problem may be to use topographically normalized reflectance instead of digital numbers (DN).

When the image is corrupted due to orthorectification, the texture may become distorted, as can be seen in Eikesdalsvatnet / Example 3 (Figure 4-4). These effects may be caused by insufficient resolution of the DEM, or by factors in the orthorectification tool which lie beyond our control, and therefore, further discussion of this problem is beyond the scope of this report.

Comparing Figure 4-5 (Eikesdalsvatnet / Example 4) to the above mentioned figures, we see that we are able to detect avalanches with different types of characteristics; the avalanche in this figure is in a very bright area surrounded by smooth snow, as opposed to the avalanches close to or inside the forest in the prior three figures. The avalanches used for training (extracted from the Hellesylt image) had a visual resemblance closer to the darker/forest type. In the Davos image A / Example 2 (Figure 4-11) and Davos image C / Example 2 (Figure 4-17) we see a third type of avalanche with darker areas of rock and soil material blended into the snow. In both examples, most of these ground avalanches have been classified as "sparse forest". Although there are no trees, it may be a positive indicator that the algorithm is able to separate avalanches

with different types of textures. A potential improvement may be to include samples from several avalanche classes in the training stage.

In the Val Gronda image we see several examples of small (in terms of extent) and relatively old avalanches, such as the ones in Val Gronda / Example 1 (Figure 4-7), which hinders successful detection, both because of the poor visibility, but also because this kind of avalanches were not represented in the training data. Davos image D / Example 1 (Figure 4-19) illustrates clearly how fresh avalanches are detected, while the older avalanche in the same image is not.

Val Gronda / Example 2 (Figure 4-8) shows a case of a false positive detection. Note the rugged snow patterns caused by ski tracks and a creek bed, running more or less in the aspect direction, having similar texture to an avalanche, which may help explain why the algorithm erroneously classifies this area.

In Davos image A / Example 1 (Figure 4-10) the algorithm is able to map the avalanches fairly well, but we also see that areas of rock have been classified as "sparse forest". The Davos landscape is in many ways different than the Hellesylt landscape (e.g., there are no forest in the Davos images), thus the method should be trained for different landscape types - including different sets of class division - in order to optimize the performance.

In general, the validation on the Davos dataset yielded better results (see especially Figure 4-10, Figure 4-16, Figure 4-17, Figure 4-19, and Figure 4-20) than what could have been expected based on the fact that both the landscape and sensor type is different from the training dataset. At the same time, it is reasonable that aerial images enhance the visibility of objects and textures (compared to satellite images), and thereby improves the result, even if the images were down-sampled to QuickBird resolution.

6 Conclusions

It was not necessarily expected that the directional filter approach would yield meaningful results if the validation image is covering a scene at another geographical location than the training image, since the vegetation and terrain may be completely different (Larsen et al., 2010), which is the case especially for both the Swiss datasets. However, the analysis on the evaluation data showed that we are able to detect several avalanche regions in images with rather different conditions, although there are still some challenges related to the segmentation.

The overall performance may be assessed as fairly good for the Eikesdalsvatnet and Davos datasets, while it is less satisfactory for the Val Gronda image. The reason may be that the Val Gronda image contains many small and old avalanches.

In the current report we have discussed several ideas for improving the avalanche detection method. Most importantly, we have considered to develop a more sophisticated normalization scheme that takes local conditions and shadows into account, and to include data from various locations into the training stage, and perhaps to define separate class division sets and/or training data bases to represent different types of image data.

So far we have only segmented the image by pixel based classification. Many of the observed avalanches contain connected regions of pixels classified as avalanche, but it still remains to solve the problem of how to combine the various connected components, i.e., to extract the shape of the avalanche. A related task concerns feature extraction of the mapped avalanche segments, and finally object classification. By combining shape related features with context related features, such as number of neighbouring objects, terrain aspect, etc., we believe that detection and mapping of avalanches could be adequately performed.

7 References

A. C. Bovik, M. Clark, and W. S. Geisler, 1990. Multichannel texture analysis using localized spatial filters. *IEEE Trans. Pattern Anal. Machin. Intell.,*vol. 12, no. 1, 55—72.

Y. Bühler, 2009. Automatisierte Erkennung und Kartierung von Lawinenablagerungen mit optischen Fernerkundungsdaten. Dissertation, Mathematisch-naturwissenschaftliche Fakultät, Universität Zürich.

Y. Bühler, A. Hüni, M. Christen, R. Meister, and T. Kellenberger, 2009. Automated detection and mapping of avalanche deposits using airborne optical remote sensing data. *Cold Regions Science and Technology*, vol. 57, pp. 99-106.

I. Fogel and D. Sagi, 1989. Gabor filters as texture discriminators. *Biol. Cybern.,* vol. 61, 103—113.

R. Frauenfelder, K. Kronholm, R. Solberg, S. Ø. Larsen, and A.-B. Salberg, 2010. avalRS – Remote sensing derived avalanche inventory data for decision support and hindcast after avalanche events. Service Demonstration Document, Deliverable 2 (D2), Project ESRIN/Contract No. 22139/08/I-EC. avalRS consortium, April 20th, 2010: 21 pp.

R. Frauenfelder, 2011. avalRS - Remote sensing derived avalanche inventory data for decision support and hindcast after avalanche events. Product Delivery Document, Deliverable 4 (D4), Project ESTRIN/Contract No. 22139/08/I-EC. avalRS consortium, June 8th, 2011: 13 pp.

R. M. Haralick, K. Shanmugam, and I. Dinstein, 1973. Textural Features for Image Classification. *IEEE Trans. Systems, Man, Cybern*., vol. 3, no. 6, pp. 610-621.

A. K. Jain, N. K. Ratha and S. Lakshmanan, 1997. Object detection using Gabor filters, *Pattern Recogn*., vol. 30(2), 293—309.

S.Ø. Larsen, H. Koren and R. Solberg, 2009. Traffic Monitoring Using Very-High-Resolution Satellite Imagery. *Photogrammetric Engineering and Remote Sensing*, vol. 75, 859-869.

S. Ø. Larsen, A. B. Salberg, and R. Solberg, 2010. Automatic detection of avalanches in high-resolution optical satellite data. Results from the ESA avalRS project's feasibility study on automated avalanche detection. *NR Note,* Norwegian Computing Center, SAMBA/04/10.

A. Solberg, C. Brekke and P. Husøy, 2007. Oil spill detection in Radarsat and Envisat SAR images, *IEEE Trans. Geosci. Remote Sens*., vol. 45, 746-755.

A. Solberg and Ø. D. Trier, 2009. SatHavOlje: Improvements during the 2008 project. *NR Note*, Norwegian Computing Center, SAMBA/01/09.

Ø.D. Trier, S.Ø. Larsen and R. Solberg, 2009. Automatic detection of circular structures in high-resolution satellite images of agricultural land. *Archaeological Prospection*, vol. 16, 1-15.

M. Varma and A. Zisserman, 2004. A statistical approach to texture classification from single images. *Int. J. Computer Vision: Special Issue on Texture Analysis and Synthesis*, vol. 62(1-2), 61—81.